Isotope shifts and hyperfine structure in near-ultraviolet transitions of Pb I by Doppler-free saturation spectroscopy

S. Bouazza,[1,*] D. S. Gough,[2] P. Hannaford,[2] R. M. Lowe,[2] and M. Wilson[3]
[1]*Département de Physique, Faculté des Sciences, Boîte Postale 1039, 51687 Reims, France*
[2]*CSIRO Manufacturing Science and Technology, Clayton, Victoria 3169, Australia*
[3]*Department of Physics, Royal Holloway College, University of London, Egham, Surrey TW20 OEX, United Kingdom*
(Received 24 July 2000; published 13 December 2000)

Isotope shifts and hyperfine structures have been determined for the three near-ultraviolet transitions 405.8 nm ($6s^26p^2\ ^3P_2-6s^26p7s\ ^3P_1^o$), 368.3 nm ($6s^26p^2\ ^3P_1-6s^26p7s\ ^3P_0^o$), and 364.0 nm ($6s^26p^2\ ^3P_1-6s^26p7s\ ^3P_1^o$) in stable isotopes of Pb I using the technique of saturated absorption spectroscopy in a sputtered vapor. The isotope shifts for these transitions and the magnetic hyperfine interaction constants for the $6s^26p^2\ ^3P_{1,2}$ metastable levels are the first Doppler-free determinations for these systems reported in the literature to our knowledge. Combined with experimental data, previously given in the literature, and pseudorelativistic Hartree-Fock estimates, the field shifts (FS's) of seven relevant configurations are deduced: FS($6s^26p7s$) = 2461 MHz, FS($6s^26p9p$) = 1838 MHz, FS($6s^26p6d$) = 1820 MHz, FS($6s^26p7d$) = 1668 MHz, FS($6s^26p8s$) = 2132 MHz, FS($6s^26p7p$) = 395 MHz, and FS($6s^26p5f$) = −461 MHz, referred to $6s^26p^2$. The hyperfine-structure integrals deduced from the experimental *A* factors for *p* electrons of the ground configuration $6s^26p^2$ are in good agreement with results of *ab initio* calculations.

DOI: 10.1103/PhysRevA.63.012516 PACS number(s): 31.30.Gs

I. INTRODUCTION

Hyperfine structures (hfs's) and isotope shifts (IS's) in Pb I have been studied extensively over the years using classical Doppler-limited and other nonlaser techniques [1–4]. However, the only laser Doppler-free studies reported to date to our knowledge have been for the $6s^26p^2\ ^3P_0-6s^26p7s\ ^3P_1^o$ resonance line at 283.3 nm [5]. The remaining transitions from the $6s^26p^2\ ^3P$ ground term are in the near-ultraviolet or far-ultraviolet region of the spectrum and are not easily accessible to narrow-bandwidth cw dye lasers.

The availability of cw titanium-sapphire lasers with frequency doubling has permitted high-power (tens of milliwatts) narrow-bandwidth laser light to be generated in the near ultraviolet and this has opened up an important spectral region not easily accessible to cw dye lasers. In this paper we report Doppler-free saturated absorption spectra for the 364.0-, 368.3-, and 405.8-nm transitions in Pb I obtained using a frequency-doubled cw titanium-sapphire ring laser. The lead vapor is generated by cathodic sputtering in a hollow-cathode discharge, which produces an adequate population of the $6s^26p^2\ ^3P_{1,2}$ metastable levels at 7819 and 10 650 cm^{-1}, respectively (Fig. 1). The saturated absorption spectra permit accurate determinations of magnetic hyperfine interaction constants for the $6s^26p^2\ ^3P_{1,2}$ and $6s^26p7s\ ^3P_0^o$ levels in ^{207}Pb ($I=\frac{1}{2}$) and of isotope shifts for the 364.0-, 368.3-, and 405.8-nm transitions. These results represent the first Doppler-free determinations of hyperfine structures for the $6s^26p^2\ ^3P_{1,2}$ metastable levels and isotope shifts for the above transitions to our knowledge.

*Email address: safa.bouazza@univ-reims.fr

II. EXPERIMENT

The experimental arrangement is shown in Fig. 2. The laser is an actively stabilized cw titanium-sapphire ring laser (Coherent 899) with an intracavity $LiIO_3$ frequency-doubling crystal. The narrow-band, frequency-doubled output of this laser is split into two counterpropagating beams, a pump beam and a weak probe beam. The pump beam is modulated at frequencies up to 300 kHz by an acousto-optic modulator;

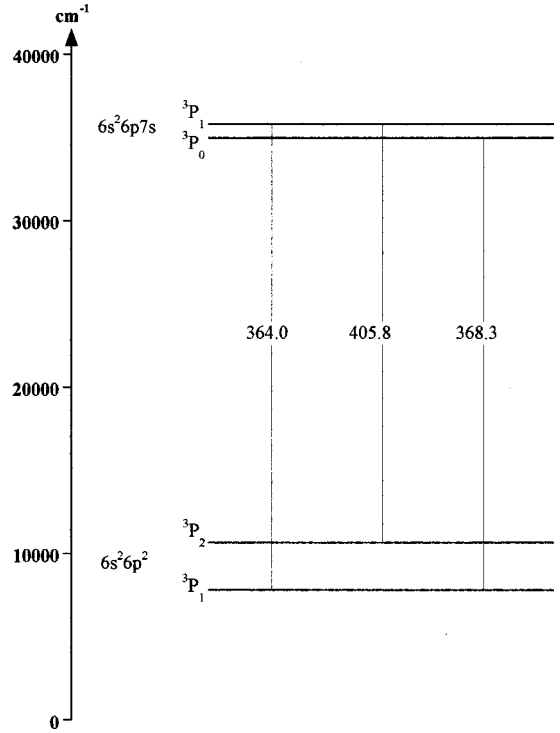

FIG. 1. Partial energy-level scheme for Pb I showing transitions (in nanometers) used in this work.

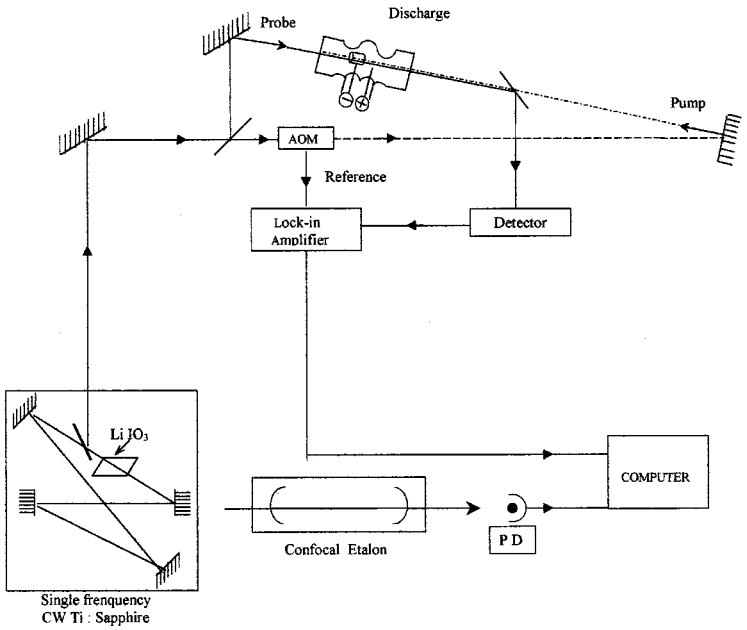

FIG. 2. Doppler-free saturated absorption setup used in this work. AOM, acousto-optic modulator; PD, photodiode.

the high frequency serving the dual purpose of suppressing pedestals arising from velocity-changing collisions between the lead and the rare-gas atoms in the discharge [6] and reducing the effect of laser noise. The transmission of the probe beam through the atomic vapor is detected by a photodiode (EG&G FND 100) and lock-in amplifier, which is referenced to the modulation frequency of the acousto-optic modulator.

The sputtering cell, which has been described in detail elsewhere [7], consists of a Pyrex chamber containing a tungsten pin anode and a lead hollow cathode (internal diameter 15 mm, length 20 mm) connected to a second tungsten pin. The hollow-cathode discharge is operated in argon at pressures of typically 0.5 Torr. Under these conditions a discharge current of only a few milliamperes is sufficient to generate an adequate concentration of metastable lower levels $6s^2 6p^2\ ^3P_1 (7810\,\mathrm{cm}^{-1})$ and $6s^2 6p^2\ ^3P_2\,(10\,650\,\mathrm{cm}^{-1})$.

Frequency calibration of the laser scans is provided by simultaneously recording fringes (at the fundamental frequency of the laser) from an external, thermally stabilized confocal étalon of length 71 cm. The free spectral range of the étalon (105.428 ± 0.012 MHz) was determined by recording saturated absorption spectra of the Yb II 369.4-nm ($6s\ ^2S_{1/2} - 6p\ ^2P_{1/2}$) transition for which the ground-state hyperfine splitting of the ^{171}Yb and ^{173}Yb components is accurately known [8,9].

To obtain a saturated absorption spectrum a voltage generated by the computer was used to scan the laser, and at the same time the analog signals produced by the amplifier and étalon were digitized and recorded in the computer. A computer program was then used to curve-fit to the data and interpolate between étalon markers. When the laser pump

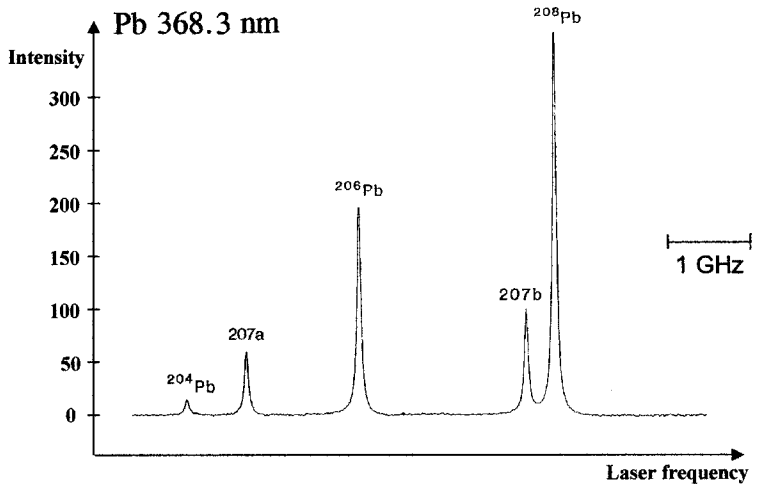

FIG. 3. Example of the recorded spectrum of the 368.3-nm line of Pb due to the transition $6s^2 6p^2\ ^3P_1 - 6s^2 6p 7s\ ^3P_0$. The laser frequency increases from left to right.

TABLE I. Results for isotope shifts of spectral lines of Pb in MHz, as deduced from experimental data.

Wavelength (nm)	Transition	$\Delta T^{204\text{-}208}$	$\Delta T^{206\text{-}208}$	$\Delta T^{207\text{-}208}$
364.0	$6p^2\ ^3P_1-6p7s\ ^3P_1$	4625.7(1.4)	2447.6(0.6)	1525.2(0.4)
368.3	$6p^2\ ^3P_1-6p7s\ ^3P_0$	4707.0(0.5)	2490.3(0.3)	1556.3(0.2)
405.8	$6p^2\ ^3P_2-6p7s\ ^3P_1$	4587.6(0.6)	2427.7(0.5)	1515.2(0.5)

TABLE II. Magnetic hyperfine structure constants A of the ^{207}Pb levels, in MHz, determined from Doppler-free saturated absorption spectroscopy.

		A			
Designation	Energy (cm^{-1})	Present work	[5]	[32]	[33]
$6s^26p^2\ ^3P_1$	7819	−2389.4(0.7)		−2388.2(4.5)	
$6s^26p^2\ ^3P_2$	10 650	2600.8(0.9)			
$6s^26p7s\ ^3P_1$	35 287	8802.0(1.6)	8807.2(3.0)		8807.2(3.0)

TABLE III. *Ab initio* data of the center-of-gravity positions (in cm^{-1}) of the low-lying even-parity configuration levels, obtained with the Cowan code [18].

$6p^2$	$6p7p$	$6p8p$	$6p5f$	$6p9p$	$6p6f$	$6p10p$	$6p7f$	$6p8f$
14 231[a]	53 404	61 235	62 301	64 382	64 851	65 992	66 245	67 109

[a]Using the relation $E_{av}=\Sigma_{levels}(2J+1)E^J/\Sigma_{levels}(2J+1)$ and considering that configuration-interaction perturbations with $6s^26p^2$ are small.

TABLE IV. Leading eigenvector components for the five ground-configuration $6s^26p^2$ levels.

		Admixture coefficients (%)					
		$6s^26p^2$			$6s^26p7p$		
E (cm^{-1}) [13]	Designation	$(^3P)^3P$	$(^1S)^1S$	$(^1D)^1D$	$(^2P)^3P$	$(^2P)^1S$	Method
0	$^3P_0$	85.9	14.1				Fit 1
		87.0	12.8				Fit 2
29 467	$^1S_0$	14.0	83.9			1.8	Fit 1
		12.8	85.0		0.8	0.6	Fit 2
7 819	$^3P_1$	100					Fit 1
		100					Fit 2
10 650	$^3P_2$	59.6		40.4			Fit 1
		62.3		37.7			Fit 2
21 458	$^1D_2$	40.4		59.6			Fit 1
		37.6		62.1			Fit 2

TABLE V. Computed and experimental radial intergrals in the $6s^26p^2$ configuration (in a.u.).

	$\langle r^{-3}\rangle^{01}$	$\langle r^{-3}\rangle^{12}$	$\langle r^{-3}\rangle^{10}$
OHFS	22.898	48.076	−8.519[a]
HF	22.302	44.390	−7.337[a]
Expt.	21.17	49.33	−15.15

[a]Relativistic part only (the contributions of spin polarization have not been taken into account).

beam is chopped at frequencies of less than 200 kHz (at the operating pressure of 0.5 Torr) the spectra of the transitions at 405.8 and 364.0 nm contain a significant background pedestal, which arises from velocity-changing collisions (VCC's) between the lead atoms and the rare-gas atoms in the discharge. At rare-gas pressures of the order of 1 Torr a sufficient number of VCC's occur during the laser-atom interaction time (given by the half period of the chopping of the pump beam or by the beam transit time, whichever is the shorter) for all velocity groups in the lower level to be coupled to the laser, and branching from the $6s^26p7s\ ^3P_1^o$ upper level to other levels not coupled to the laser can cause severe depletion of the $6s^26p^2\ ^3P_2$ or $6s^26p^2\ ^3P_1$ lower-level population over the entire velocity distribution. At low chopping frequencies there is sufficient time during the off part of the pump-beam chopping cycle for the lower level to be replenished by diffusion of fresh lead atoms into the interaction region, and the saturated absorption signal (which is the difference in probe laser transmission with the pump beam on and off) exhibits very large VCC pedestals. At high chopping frequencies (>200 kHz), where there is less time for replenishment of the lower-level atoms, the atomic system remains optically pumped throughout the chopping cycle, and the VCC signals are small [10,11].

Figure 3 shows a saturated absorption spectrum of the 368.3-nm transition. The observed linewidth of the individual components is about 60 MHz (full width at half maximum [FWHM]). For this transition, the natural width is 22 MHz [12]. Measurements of the linewidth as a function of argon pressure and of laser power indicate that the contributions of power broadening and pressure broadening are about 20 and 10 MHz, respectively. Laser jitter is estimated to contribute about 5 MHz to the total linewidth.

The isotope shift data in Table I represent the means of typically 15 spectra and the uncertainties quoted include contributions from the uncertainty in the free spectral range of the étalon. These Doppler-free isotope shift data represent an improvement in accuracy of about an order of magnitude over earlier Doppler-limited results. The hyperfine interaction constants (Table II) were derived from transitions relevant to each level: $6s^26p^2\ ^3P_1$ (7819 cm^{-1}) from 368.3 and 364.0 nm; $6s^26p^2\ ^3P_2$ (10 650 cm^{-1}) from 405.8 nm; and $6s^26p7s\ ^3P_1^o$ (35 287 cm^{-1}) from 364.0 and 405.8 nm. The magnetic hyperfine interaction constants reported here for the $6s^26p^2\ ^3P_{1,2}$ levels represent an improvement in accuracy of an order of magnitude over previous work. For the other level ($6s^26p7s\ ^3P_1^o$), our results are in good agreement with those of Thompson *et al.* [5].

TABLE VI. Vinti integral k factors (in a.u.) as defined in [18,24].

Configuration	k factor −7912
$6p7s$	0.6595
$6p8s$	0.6213
$6p9s$	0.6134
$6p6d$	0.6111
$6p7d$	0.6084
$6p8d$	0.6079
$6p^2$	0.7779
$6p7p$	0.6198
$6p8p$	0.6114
$6p5f$	0.6073
$6p9p$	0.6093
$6p6f$	0.6073
$6p10p$	0.6085

III. DISCUSSION OF RESULTS

A. Wave functions

The energy levels of Pb I compiled in [13] are based on the extensive analysis by Gieseler and Grotrian [14] with many additions and improvements from the work of Meggers [15], who utilized spectrograms furnished by Shenstone.

More recently a complete interpretation of the 51 odd-parity configuration levels of Pb I was achieved [16], using all data available from absorption and emission spectroscopy measurements, photoionization experiments, and ejected electron spectroscopy. As regards even-parity levels Wood and Andrew [17] reinvestigated the Pb I emission spectrum with improved and accurate wavelengths and determined energies of 59 levels. Unfortunately, apart from this uncompleted work, very few details have been reported in the literature.

The $6s^26p^2$ ground configuration of Pb I gives rise to the five levels $^1D_2$, $^3P_{2,1,0}$, and $^1S_0$ which, except the last, are probably not severely affected by mixing with levels of higher-lying configurations since they are located quite far from any such. In Table III we give *ab initio* evaluations of the center-of-gravity positions of the low-lying even-parity configuration levels, performed with the Cowan code [18]. One can note, for example, that strong configuration interactions are expected between $6s^26pnp$ and $6s^26p(n-2)f$ ($n=7,8,9,10$).

TABLE VII. Calculated specific mass shifts in MHz for Pb transitions under study.

Transition	ΔT_{SMS}
$6p^2$-$6p7s$	−20.0
$6p^2$-$6p6d$	−28.1
$6p^2$-$6p7d$	−28.6
$6p^2$-$6p8s$	−26.4
$6p7s$-$6p9p$	−8.5
$6p7s$-$6p8p$	−8.1

TABLE VIII. Results of the separation of SMS and FS in MHz for isotope pair 206-208 for lines under study. PW indicates present work. NMS indicates normal mass shift.

λ (nm)	Classification	Expt. $\Delta T^{206\text{-}208}$	Ref.	NMS	SMS	FS
402.0	$6p^2\ ^1D_2-6p6d\ ^3F_3$	1836	[2]	19.1	−28.1	1845
406.2	$6p^2\ ^1D_2-6p6d\ ^3D_1$	1851	[2]	18.9	−28.1	1860
434.0	$6p^2\ ^1S_0-6p7d\ ^3D_1$	1692	[2]	17.7	−28.6	1703
500.7	$6p7s\ ^3P_0-6p9p\ ^3P_1$	−540	[2]	15.4	−8.5	−547
520.1	$6p^2\ ^1S_0-6p8s\ ^3P_1$	2097	[2]	14.8	−26.4	2110
589.6	$6p7s\ ^3P_0-6p8p\ ^3P_1$	−783	[2]	13.0	−8.1	−788
601.2	$6p7s\ ^3P_1-6p8p\ ^3P_1$	−780	[2]	12.8	−8.1	−785
605.9	$6p7s\ ^3P_1-6p8p\ ^3P_0$	−780	[2]	12.7	−8.1	−784
722.9	$6p^2\ ^1D_2-6p7s\ ^3P_1$	−2713	[26]	10.6	−20.0	−2704
283.3	$6p^2\ ^3P_0-6p7s\ ^3P_1$	−2227	[5,25]	27.1	−20.0	−2234
364.0	$6p^2\ ^3P_1-6p7s\ ^3P_1$	−2448	PW	21.1	−20.0	−2449
368.3	$6p^2\ ^3P_1-6p7s\ ^3P_0$	−2490	PW	20.9	−20.0	−2491
405.8	$6p^2\ ^3P_2-6p7s\ ^3P_1$	−2428	PW	18.9	−20.0	−2427

We fitted the five experimental ground configuration levels taking into account the terms of the closest configuration, $6s^26p7p$ (fit 1, Table IV); the leading eigenvector components for the ground configuration levels are given, together with the results of relativistic Hartree-Fock calculations, considering the basis set of the following seven configurations: $6s^26p^2$, $6s^26p7p$, $6s^26p8p$, $6s^26p9p$, $6s^26p5f$, $6s^26p6f$, $6s^26p10p$ (fit 2). Unfortunately the insufficient number of experimental energy levels for this basis set makes their straightforward fitting presently impossible to perform (since there are distinctly more parameters to determine than available energy levels).

B. Hyperfine-structure analysis

1. hfs parameter coefficients in intermediate coupling

As can be seen from Table IV there are no significant differences between eigenvector components obtained by fit 1 or fit 2. The wave functions of hfs interest in intermediate coupling can be expressed in terms of the *LS* and *jj* coupled basis sets:

$$|^3\hat{P}_1\rangle = |^3P_1\rangle$$

$$|^3\hat{P}_2\rangle = -0.636|^1D_2\rangle + 0.772|^3P_2\rangle$$
$$= 0.263|\tfrac{3}{2},\tfrac{3}{2},2\rangle + 0.965|\tfrac{3}{2},\tfrac{1}{2},2\rangle,$$

$$|^1\hat{D}_2\rangle = 0.772|^1D_2\rangle + 0.636|^3P_2\rangle$$
$$= 0.965|\tfrac{3}{2},\tfrac{3}{2},2\rangle - 0.263|\tfrac{3}{2},\tfrac{1}{2},2\rangle.$$

Since the nuclear spin of ^{207}Pb is equal to $\frac{1}{2}$ there is only the magnetic hfs splitting factor A to consider. The expansions of the magnetic hfs factor A in intermediate coupling are shown directly as follows:

$$A(^3P_1) = 0.5a^{01} + 0.5a^{10} - 0.5a^{12} = -2389.4 \text{ MHz}, \quad (1)$$

$$A(^3P_2) = 0.702a^{01} + 0.298a^{10} + 0.268a^{12} = 2600.8 \text{ MHz}, \quad (2)$$

$$A(^1D_2) = 0.797a^{01} + 0.202a^{10} - 0.168a^{12} = 609.82 \text{ MHz}, \quad (3)$$

where experimental values are taken from Table II and from [26].

2. Monoelectronic hfs constants

Different methods have already been used to calculate the $6s^26p^2$ configuration radial integrals $\langle r^{-3}\rangle^{\kappa k}$ for p electrons. In this work we have chosen the results obtained by Hartree-Fock (HF) and optimized Hartree-Fock-Slater (OHFS) methods [19]: these are listed in Table V, in which we have included for comparison the experimental values deduced when solving Eqs. (1)–(3) and using the relation

$$a^{\kappa k} = 95.4128(\mu_N/I)\langle r^{-3}\rangle^{\kappa k}$$

with $\mu_N = 0.5783$ [20]. We note that in this Table V the computed and measured values of $\langle r^{-3}\rangle^{10}$ are different. The computed value stands for the relativistic contributions whereas the measured value also takes into account the effects of spin polarization due to the interactions with unknown configurations; an educated guess might be $6sns6p^2$ with $n \geqslant 7$:

$$\langle r^{-3}\rangle^{10}_{\text{expt}} = \langle r^{-3}\rangle^{10}_{\text{relat}} + \langle r^{-3}\rangle^{10}_{\text{polar}}.$$

We showed in previous work [21] that the fraction of the spin polarization is 50.62% in the case of Bi II, which is isoelectronic with Pb I; and if we assume the effect to be of comparable percentage then the mean corrected value of $\langle r^{-3}\rangle^{10}$ is $(-8.519-7.337)/2\times 0.4938 = -16.06$ a.u., which is in reasonable agreement with the experimental value.

TABLE IX. PSUHFR values of total electron densities at the nucleus, $4\pi|\psi(0)|^2$, in a.u.

Configuration	$4\pi\|\psi(0)\|^2-26\,629\,000$
$6s^26p7s$	998
$6s^26p6d$	782
$6s^26p7d$	724
$6s^26p9p$	776
$6s^26p8p$	882
$6s^26p7p$	290
$6s^26p^2$	161
$6s^26p5f$	−2

C. Isotope shifts

Since the early days of spectroscopy lead has been of particular interest in isotope shift studies, which can yield information on the behavior of nuclear radii in the region of the doubly magic nucleus ^{208}Pb. It is considered as a heavy element for which it can often be assumed that the isotope shifts are predominantly caused by the volume effect [22].

On the other hand, King [23] showed that the so-called specific mass shifts may be non-negligible in heavy elements when certain electron-electron correlation effects assume importance. So we propose first to estimate the effects of the specific mass shift (SMS) contributions, resorting to the use of *ab initio* calculations.

1. Ab initio estimates of k

It has been known for some time that the Hartree-Fock wave functions can provide realistic indications of the detailed behavior of the field and specific mass contributions to the observed isotope shifts [24]. Since Pb ($Z=82$) has a high atomic number, to ensure that relativistic effects are allowed for we consider only results obtained using the pseudorelativistic Hartree-Fock (HFR) model. Use of the Cowan code [18] gives the total Vinti integral contributions k (in atomic units) presented in Table VI; from these k values one can deduce estimates of the SMS, ΔT_{SMS} (in MHz), which are given in Table VII for the transitions under study here. In this work we assume that all terms of the same configuration possess the same SMS contribution since, for example, $k(6s^26p7s\ ^3P)-k(6s^26p7s\ ^1P)\cong 0.001$ a.u., i.e., less than 1 MHz between the isotopes 206 and 208.

TABLE X. The two mean eigenvector components for the levels involved in the IS study.

Term	First component (%)	Second component (%)	Reference
$6p7s\ ^3P_0$	99.5 $6p7s\ ^3P$	0.2 $6p8s\ ^3P$	[16]
$6p7s\ ^3P_1$	70.2 $6p7s\ ^3P$	26.8 $6p7s\ ^1P$	[16]
$6p7s\ ^1P_1$	48.7 $6p7s\ ^1P$	21.5 $6p7s\ ^3P$	[16]
$6p6d\ ^3D_1$	48.4 $6p6d\ ^3D$	26.8 $6p6d\ ^1P$	[16]
$6p6d\ ^3F_3$	48.8 $6p6d\ ^3F$	26.9 $6p6d\ ^1F$	[16]
$6p8s\ ^3P_1$	57.4 $6p8s\ ^3P$	26.7 $6p8s\ ^1P$	[16]
$6p9p\ ^3P_0$	65.3 $6p9p\ ^3P$	24.1 $6p9p\ ^1S$	*ab initio* [18]
$6p8p\ ^3P_0$	66.7 $6p8p\ ^3P_0$	24.6 $6p8p\ ^1S$	*ab initio* [18]

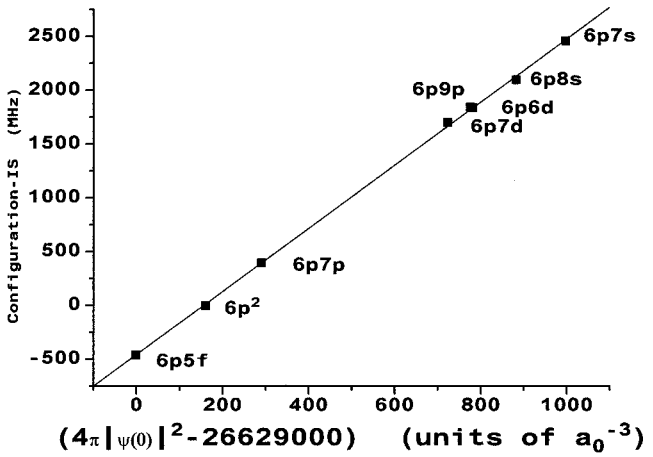

FIG. 4. ΔT (in MHz) for Pb I versus PSUHFR values of $4\pi|\psi(0)|^2-26\,629\,000$ (in a.u.).

2. Evaluation of field and configuration isotope shifts

(a) Experimental data. Selected best available experimental isotope shift data for Pb, $\Delta T^{206\text{-}208}$, taken from the literature are presented in Table VIII together with those of the present work. From the old (Doppler-limited) but excellent work of Blaise [2] we deduce that $\Delta T^{206\text{-}208}=1840$ MHz between $6s^26p^2$ and $6s^26p6d$ configurations, $\Delta T^{206\text{-}208}=-785$ MHz between $6s^26p7s$ and $6s^26p8p$, $\Delta T^{206\text{-}208}=2110$ MHz between $6s^26p^2$ and $6s^26p8s$, $\Delta T^{206\text{-}208}=1703$ MHz between $6s^26p^2$ and $6s^26p7d$, and $\Delta T^{206\text{-}208}=-547$ MHz between $6s^26p7s$ and $6s^26p9p$; and from the work of Thompson *et al.* [5], Moscatelli *et al.* [25], Dinger *et al.* [26], and the present work, $\Delta T^{206\text{-}208}=2461$ MHz between $6s^26p^2$ and $6s^26p7s$.

(b) Ab initio calculations. The method of calculation used to obtain the results in this work is based on the so-called pseudorelativistic Hartree-Fock (PSUHFR) procedure whose usefulness for the interpretation of isotope shift stud-

TABLE XI. Theoretical and experimental configuration IS values in Pb I. PW indicates present work.

Configuration	Total HFR[a]	ΔT_{expt} (MHz)	$\Delta T_{\mathrm{theor}}$ (MHz)	Reference
$6s^26p^2$	160	0[b]	0[b]	
$6s^26p7s$	998	2461[b]	2461[b]	[5], [25], [26], PW
$6s^26p9p$	782	1840	1838	[5]
$6s^26p7d$	724	1703	1668	[5]
$6s^26p6d$	776	1843	1820	[5]
$6s^26p8s$	882	2097	2132	[5]
$6s^26p5f$	−2		−461	
$6s^26p7p$	290		395	

[a]Plus an additional constant of $26\,629\,000a_0^{-3}$.
[b]Experimental IS values used for calibration in Fig. 3.

ies has been tested on Ce II [27], Re I [28,29], and Hf [30]. This procedure, based on the Froese-Fischer code [31], includes, as in the Cowan code, the mass-velocity and Darwin terms of the Pauli approximation in the usual nonrelativistic Hartree-Fock Hamiltonian. This has the effect of reproducing the main effects of relativity in that the charge-density distributions are much closer to those obtained from Dirac-Fock calculations than those from HF calculations.

Single-configuration PSUHFR calculations were made for the following configurations of Pb I: $6s^2 6p 7s$, $6s^2 6p 6d$, $6s^2 6p 7d$ (odd) and $6s^2 6p 9p$, $6s^2 6p 8p$, $6s^2 6p 7p$, $6s^2 6p^2$, and $6s^2 6p 5f$ (even). The resulting values of electron density at the nucleus, $4\pi|\psi(0)|^2$, are given in Table IX. We have used the PSUHFR values of $4\pi|\psi(0)|^2$ and the experimental values of ΔT for $6s^2 6p^2$ and $6s^2 6p 7s$ configurations, which are considered pure (see Tables IV and X), to calibrate our calculations and construct the straight line [29,30], shown in Fig. 4. From this graph, theoretical isotope shifts of the main Pb I configurations were obtained and compared with experimental data (Table XI).

IV. CONCLUSION

Doppler-free saturated absorption spectroscopy measurements of Pb I in the near ultraviolet were reported. Additional levels were then accessible to laser spectroscopy and the accuracy of some previously obtained experimental data was improved. Pb I and Pb II have historically played an important role in understanding basic phenomena in isotope shift studies. We confirm once more that the isotope shifts are predominantly caused by the volume effect, even for transitions involving a *d* electron (see Table VII). We give the theoretical field shifts (FS's) of the main configurations: $\mathrm{FS}(6s^2 6p 7s) = 2461\,\mathrm{MHz}$, $\mathrm{FS}(6s^2 6p 9p) = 1838\,\mathrm{MHz}$, $\mathrm{FS}(6s^2 6p 6d) = 1820\,\mathrm{MHz}$, $\mathrm{FS}(6s^2 6p 7d) = 1668\,\mathrm{MHz}$, $\mathrm{FS}(6s^2 6p 8s) = 2132\,\mathrm{MHz}$, $\mathrm{FS}(6s^2 6p 7p) = 395\,\mathrm{MHz}$, and $\mathrm{FS}(6s^2 6p 5f) = -461\,\mathrm{MHz}$, referred to $6s^2 6p^2$.

[1] P. Brix and H. Kopfermann, in *Numerical Data and Functional Relationships in Science and Technology*, Landolt-Börnstein, New Series, Group I, Vol. 5 (Springer-Verlag, Berlin, 1952), and references therein.
[2] J. Blaise, Ann. Phys. (Paris) **3**, 1019 (1958).
[3] P. L. Larkins, Spectrochim. Acta, Part B **39**, 1365 (1984).
[4] E. B. Soloman and W. Happer, Phys. Rev. **144**, 7 (1966).
[5] R. C. Thompson, M. Anselment, K. Bekk, S. Goring, A. Hanser, G. Meise, H. Rebel, G. Schatz, and A. Brown, J. Phys. G **9**, 443 (1983). See also R. C. Thompson *et al.*, Z. Phys. A **305**, 89 (1982).
[6] D. S. Gough and P. Hannaford, Opt. Commun. **67**, 209 (1988).
[7] P. Hannaford, Contemp. Phys. **24**, 251 (1983).
[8] R. Casdorff, V. Enders, R. Blatt, W. Neuhauser, and P. Toschek, Ann. Phys. (Leipzig) **48**, 41 (1991).
[9] A. Münch, M. Berkler, Ch. Gerz, D. Wilsdorf, and G. Werth, Phys. Rev. A **35**, 4147 (1987).
[10] A. P. Willis, D. S. Gough, P. Hannaford, R. M. Lowe, R. J. McLean, and A. Wännstrom, in *Laser Spectroscopy X*, edited by M. Ducloy, E. Giacobino, and G. Camy (World Scientific, Singapore, 1992), p. 404.
[11] P. Hannaford and D. S. Gough (unpublished).
[12] V. N. Gorshkov and Ya. F. Verolainen, Opt. Spectrosk. **58**, 1385 (1985) [Opt. Spectrosc. **58**, 849 (1985)].
[13] C. E. Moore, *Atomic Energy Levels*, Natl. Bur. Stand. (U.S.) Circ. No. 467 (U.S. GPO, Washington, DC, 1958), Vol. III.
[14] H. Gieseler and W. Grotrian, Z. Phys. **34**, 374 (1929).
[15] W. F. Meggers (unpublished).
[16] J. Dembczynski, E. Stachowska, M. Wilson, P. Buch, and W. Ertmer, Phys. Rev. A **49**, 745 (1994).
[17] R. D. Wood and K. L. Andrew, J. Opt. Soc. Am. **58**, 818 (1968).
[18] R. D. Cowan, *The Theory of Atomic Structure and Spectra* (University of California Press, Berkeley, 1981).
[19] I. Lindgren and A. Rosen, Case Stud. At. Phys. **4**, 199 (1974).
[20] G. H. Fuller, J. Phys. Chem. Ref. Data **5**, 835 (1976).
[21] S. Bouazza and J. Bauche, Z. Phys. D: At., Mol. Clusters **10**, 1 (1988).
[22] S. Bouazza, Y. Guern, and J. Bauche, J. Phys. B **19**, 1881 (1986).
[23] W. H. King, *Isotope Shifts in Atomic Spectra* (Plenum, New York, 1984).
[24] J. Bauche and R. J. Champeau, Adv. At. Mol. Phys. **12**, 39 (1976).
[25] F. A. Moscatelli, O. Redi, P. Schönberger, H. H. Stroke, and R. I. Wiggins, J. Opt. Soc. Am. **72**, 918 (1982).
[26] U. Dinger, J. Eberz, G. Huber, R. Menges, S. Schröder, R. Kirchner, O. Klepper, T. Kühl, D. Marx, and G. D. Sprouse, Z. Phys. A **328**, 253 (1987).
[27] M. Wilson, Physica B & C **95C**, 129 (1978).
[28] M. Wilson, Phys. Lett. A **125**, 205 (1987).
[29] H.-D. Kronfeldt, D. Ashkenasi, G. Basar, L. Neale, and M. Wilson, Z. Phys. D: At., Mol. Clusters **25**, 185 (1993).
[30] S. Bouazza and M. Wilson, J. Phys. B **33**, 933 (2000).
[31] C. Froese-Fischer, *The Hartree-Fock Method for Atoms* (Wiley, New York, 1977).
[32] J. M. Reeves and E. N. Fortson, Phys. Rev. A **44**, R1439 (1991).
[33] M. Anselment, W. Faubel, S. Göring, A. Hanser, G. Meisel, H. Rebel, and G. Schatz, Nucl. Phys. A **451**, 471 (1986).